UTMS 2009–9 May 12, 2009

Conditional stability and numerical reconstruction of initial temperature

by

Jingzhi Li, Masahiro Yamamoto,
and Jun Zou

UNIVERSITY OF TOKYO
GRADUATE SCHOOL OF MATHEMATICAL SCIENCES
KOMABA, TOKYO, JAPAN

CONDITIONAL STABILITY AND NUMERICAL RECONSTRUCTION OF INITIAL TEMPERATURE

Jingzhi Li

Department of Mathematics, The Chinese University of Hong Kong
Shatin, N.T., Hong Kong, P. R. China

Masahiro Yamamoto

Department of Mathematical Sciences, The University of Tokyo
Komaba Meguro, Tokyo 153-8914, Japan

Jun Zou

Department of Mathematics, The Chinese University of Hong Kong
Shatin, N.T., Hong Kong, P. R. China

Abstract. In this paper, we address an inverse problem of reconstruction of the initial temperature in a heat conductive system when some measurement data of temperature are available, which may be observed in a subregion inside or on the boundary of the physical domain, along a time period which may start at some point, possibly far away from the initial time. A conditional stability estimate is first achieved by the Carleman estimate for such reconstruction. Numerical reconstruction algorithm is proposed based on the output least-squares formulation with the Tikhonov regularization using the finite element discretization, and the existence and convergence of the finite element solution are presented. Numerical experiments are carried out to demonstrate the applicability and effectiveness of the proposed method.

1. **Introduction.**

Consider the heat conduction equation

$$y_t = A(x)\,y \quad \text{in } \Omega \times (0,T)\,; \qquad y = 0 \quad \text{on } \partial\Omega \times (0,T), \tag{1.1}$$

where Ω is a bounded domain in $\mathbb{R}^N$ $(N = 2, 3)$ with smooth boundary $\partial\Omega$, and $A(x)$ is a second order self-adjoint elliptic operator of the form

$$A(x)\,y = \sum_{i=1}^{n}\sum_{j=1}^{n} \frac{\partial}{\partial x_i}\left(a_{ij}(x)\frac{\partial y}{\partial x_j}\right) - c(x)\,y \tag{1.2}$$

2000 *Mathematics Subject Classification.* Primary: 65N30; Secondary: 35R30.

Key words and phrases. Carleman estimate, conditional stability, backward heat problem, output least-squares, Tikhonov regularization, finite element method.

The work of the second author was partly supported by the grant 15340027 from the Japan Society for the Promotion of Science and the grant 17654019 from the Ministry of Education, Cultures, Sports and Technology. The work of the third author was substantially supported by Hong Kong RGC grants (Project 404105 and Project 404606) and partially supported by Cheung Kong Scholars Programme through Wuhan University.

where the coefficient $c(x)$ is in $L^\infty(\Omega)$ and $c(x) \geq 0$ for *a.e.* $x \in \Omega$, while the coefficients $a_{ij}(x) \in C^1(\bar{\Omega})$ satisfy that $a_{ij} = a_{ji}$ for $i, j = 1, 2, \cdots, n$ and

$$\alpha_0 \, \xi^T \xi \leq \sum_{i=1}^n \sum_{j=1}^n a_{ij}(x) \xi_i \xi_j \quad \forall\, x \in \Omega\,,\ \xi \in \mathbb{R}^n$$

for some constant $\alpha_0 > 0$.

The main interest of this paper is to investigate the theoretical and numerical possibility of the reconstruction of the initial temperature in the heat conductive system (1.1) from partial measurement data in a subregion inside or on the boundary of the physical domain, along a time period which may start at some point, possibly far away from the initial time. This problem is important to various industrial purposes, for example, effective monitoring techniques for heat conductive processes in steel industries, glass and polymer forming and nuclear power station. On the other hand, from the mathematical point of view, this problem is ill-posed in the sense of Hadamard [3], that is, small noise in data may cause huge errors in the initial temperature. However such instability may be restored in many cases by taking into consideration practically acceptable a priori assumptions for the solutions. As a typical example, we can refer to the backward heat conduction problem with a priori boundedness of solutions, where we would like to determine the initial data profile from the temperature distribution measured at a positive moment. The backward heat conduction problem with a priori boundedness can become stable, and in that case, the a priori boundedness may be interpreted as the melting point of the material under consideration.

More specifically, we shall be interested in the following two inverse problems:

Inverse Problem I. Let ω be an arbitrary subdomain of Ω, and $\tau > 0$ be a fixed constant. The inverse problem is to reconstruct the initial temperature $y(\cdot, 0)$, when the measurement data of y in $\omega \times (\tau, T)$ are available.

Inverse Problem II. Let Γ be an arbitrary fixed relatively open subset of $\partial\Omega$, and $\tau > 0$ be a fixed constant. The inverse problem is to reconstruct the initial temperature $y(\cdot, 0)$, when the measurement data of $\partial_\nu y$ in $\Gamma \times (\tau, T)$ are available, where ν is the unit outward normal to $\partial\Omega$.

Before our theoretical investigation in Section 2, we would first comment on the significance of the conditional stability from a general point of view. The conditional stability estimates can be stated as follows:

$$\|\text{deviations of solutions}\| \leq C \begin{cases} \|\text{errors in data}\| & \text{(Lipschitz-type stability)}, \\ \|\text{errors in data}\|^\alpha & \text{(Hölder-type stability)}, \\ \frac{1}{-\log \|\text{errors in data}\|} & \text{(logarithmic-type stability)} \end{cases}$$

for some generic constant C and $\alpha \in (0, 1)$, provided that deviations in solutions are assumed to be in the so-called admissible set $\mathcal{A}$. An admissible set is usually defined to be a bounded set in some appropriate function space. From the mathematical point of view, a conditional stability of logarithmic-type is much worse than the Lipschitz-type stability.

Conditional stability is not only interesting from the viewpoint of mathematical theory, but it may also provide some insightful guidance to numerical solutions of practical inverse problems. For example, rates of conditional stabilities may lead to optimal or quasi-optimal choices of the Tikhonov regularizing parameters and discretization mesh sizes, see, e.g., Cheng, Yamamoto and Zou [2], Klibanov [6] (Theorem 5), Klibanov and Timonov [7](section 2.5).

However, the rate of a conditional stability may heavily depend on the choice of admissible set $\mathcal{A}$, and different choices may improve the rate drastically. Even if one achieves only the logarithmic-type stability, it does not necessarily mean the actual poor performance of the numerical reconstruction, because the established stability estimate does not imply the logarithmic rate for actually accessible observation data in the numerics, see, e.g., the numerical tests in Yamamoto and Zou [18]. On the other hand, even if one can build up the conditional stability of Lipschitz-type, it does not always mean a satisfactory performance of the numerical solutions, since the constants involved in the conditional stability estimate may be extremely large in comparison with the noise level in the observation data.

In general, conditional stability may provide some very useful guidance for numerical computations (see, e.g., [2]). But on the other hand, one should not take the stability estimate as an absolute criterion. In this sense, the conditional stability which we shall establish in this work may not be the best, while further improvements can be expected.

As far as the ill-posed heat conduction problem is concerned, a lot of studies can be found in the literature on its conditional stability. But there are several important cases, where such stability estimates are still missing. For example, all the existing studies required the measurement data of temperatures on the time-space domain $\omega \times (0, T)$. But the measurement data up to the initial time may be very hard or impossible to achieve technically in many applications. The aim of the current work is to relax the requirement on the data. We shall establish a conditional stability estimate for the reconstruction of the initial temperature profile in the entire physical domain by means of the measurement data, observed in a subregion inside or on the boundary of the physical domain, along a time period which may start at some point, possibly far away from the initial time. To our best knowledge, our early work [19] seems to be the first investigation on the reconstruction of the initial temperature in the entire physical domain, which does not require all measurement data for a time period up to the initial time. The stability of Inverse Problem I with the interior measurement data was treated in [19] when the operator A in (1.1) is the simple Laplacian, but only with some major ideas sketched. The current work will establish the stability for both Inverse Problem I (with interior measurement data) and Inverse Problem II (with boundary measurement data) for general parabolic equation (1.1), and propose some finite element method for the numerical reconstruction of initial temperature and present many different numerical experiments to demonstrate the effectiveness and robustness of the finite element method.

The rest of the work is organized as follows. In Section 2, we establish the conditional stability estimates by taking advantage of a Carleman estimate for **Inverse Problems I** and **II** posed earlier in this section. In Section 3, we propose a numerical reconstruction method for the initial temperature, which is based on the output least-squares formulation with Tikhonov regularization using the finite element discretization, and the existence of discrete minimizers and convergence of the finite element approximation are also shown in that section. In Section 4, five concrete numerical examples of the reconstruction of the initial temperature are presented. Some interesting observations are highlighted in those tests.

2. **Conditional stability of the inverse problems.** For any fixed $\varepsilon > 0$ and $M > 0$, we introduce an admissible set by

$$\mathcal{A} = \Big\{ a \in H^{2\varepsilon}(\Omega);\ \|a\|_{H^{2\varepsilon}(\Omega)} \le M \Big\}. \tag{2.1}$$

Then the following theorem gives the first main result of this paper about the conditional stability of **Inverse Problem I**.

Theorem 2.1. Let $y(x,t)$ be the solution to the heat equation (1.1). Then for any $y(\cdot,0) \in \mathcal{A}$, there exists a constant $\kappa = \kappa(M,\varepsilon) \in (0,1)$ such that

$$\|y(\cdot,0)\|_{L^2(\Omega)} \le C(M,\varepsilon)\Big(-\log \|y\|_{L^2(\omega\times(\tau,T))}\Big)^{-\kappa}. \tag{2.2}$$

Proof. Without loss of generality, we may assume that $\|y\|_{L^2(\omega\times(\tau,T))}$ is sufficiently small, and will carry out the proof in three steps.

Step 1: application of a Carleman estimate. We first show for any fixed $\theta \in (\tau,T)$, we can choose constants $C = C(M) > 0$ and $\kappa_1 \in (0,1)$ such that

$$\|y(\cdot,\theta)\|_{L^2(\Omega)} \le C\|y\|^{\kappa_1}_{L^2(\omega\times(\tau,T))}. \tag{2.3}$$

If this is true, we can then assume that $\|y(\cdot,\theta)\|_{L^2(\Omega)} < 1$ since $\|y\|_{L^2(\omega\times(\tau,T))}$ is sufficiently small.

To prove (2.3), we first introduce some weight functions

$$\phi(x,t) = \frac{\exp(\lambda\psi(x))}{(t-\tau)(T-t)}, \quad \alpha(x,t) = \frac{\exp(\lambda\psi(x)) - \exp(2\lambda\|\psi\|_{C(\bar\Omega)})}{(t-\tau)(T-t)},$$

where $\psi(x)$ is an appropriately chosen positive function in Ω (see [4]). Then following the Carleman estimates in [4] (Theorem 2.1) for the solution $y(x,t)$ to (1.1), one can show that there exists some constant $s_0 > 0$ such that the following estimate holds for all $s \ge s_0$ and $(x,t) \in \Omega \times (\tau,T)$:

$$\int_\tau^T \int_\Omega \Big(\frac{1}{s\phi}|\nabla y|^2 + s\,\phi\, y^2\Big)e^{2s\,\alpha}dxdt \le C\int_\tau^T\int_\omega s\,\phi\, y^2 e^{2s\,\alpha}dxdt\,. \tag{2.4}$$

Now for any two arbitrarily fixed θ_1, θ_2 with $\tau < \theta_1 < \theta_2 < T$, we can easily see that

$$\phi e^{2s\,\alpha} \le \tilde C \ \text{ for } (x,t) \in \omega\times(\tau,T)\,;\ \phi e^{2s\,\alpha} \ge \tilde c\,,\ \phi^{-1}e^{2s\,\alpha} \ge \tilde c \ \text{ for } (x,t) \in \Omega\times(\theta_1,\theta_2)$$

for two positive constants $\tilde C$ and $\tilde c$ which depend only on τ, T, θ and θ_2. Then it follows readily from (2.4) that

$$\|y\|_{L^2(\theta_1,\theta_2;H^1(\Omega))} \le C_M\|y\|_{L^2(\omega\times(\tau,T))}. \tag{2.5}$$

On the other hand, multiplying both sides of equation (1.1) by any $v \in H^1_0(\Omega)$, we derive

$$\int_\Omega y_t\, v dx = -\int_\Omega \sum_{i,j=1}^n a_{ij}\frac{\partial y}{\partial x_i}\frac{\partial v}{\partial x_j}\,dx - \int_\Omega c(x) y v\,dx \quad \forall\, v \in H^1_0(\Omega),$$

which with (2.5) gives

$$\|y_t\|_{L^2(\theta_1,\theta_2;H^{-1}(\Omega))} \le C\|y\|_{L^2(\theta_1,\theta_2;H^1(\Omega))} \le C_M\|y\|_{L^2(\omega\times(\tau,T))}. \tag{2.6}$$

Therefore, by the Sobolev embedding, we obtain from (2.5) and (2.6) that

$$\|y\|_{C([\theta_1,\theta_2];H^{-1}(\Omega))} \le C_M\|y\|_{L^2(\omega\times(\tau,T))}. \tag{2.7}$$

Furthermore, by the semigroup theory (cf. Pazy [13]), we have $y(t) = y(\cdot,t) = e^{tA}y(\cdot,0)$, where A is the elliptic operator defined in (1.2) with $\mathcal{D}(A) = H_0^1(\Omega) \cap H^2(\Omega)$. Then for any $\gamma > 0$, there exists a constant $C_\gamma > 0$ such that (cf. [13])

$$\|(-A)^\gamma e^{tA}\| \le C_\gamma t^{-\gamma}, \quad \|a\|_{H^{2\gamma}(\Omega)} \le C_\gamma \|(-A)^\gamma a\|_{L^2(\Omega)}\,. \tag{2.8}$$

This implies

$$\begin{aligned} \|y\|_{C([\theta_1,\theta_2];H^{2\gamma}(\Omega))} &\le C_\gamma \|(-A)^\gamma e^{tA} y(\cdot,0)\|_{C([\theta_1,\theta_2];L^2(\Omega))} \\ &\le \frac{C_\gamma}{\theta_1^\gamma}\|y(\cdot,0)\|_{L^2(\Omega)} \le \frac{C_\gamma M}{\theta_1^\gamma}. \end{aligned} \tag{2.9}$$

Then by the interpolation theory (e.g., Proposition 2.3 (p.19) and Theorem 12.4 (p.73) in Lions and Magenes [11]), (2.7) and (2.9) yield

$$\begin{aligned} \|y\|_{C([\theta_1,\theta_2];L^2(\Omega))} &\le \|y\|^{\frac{2\gamma}{2\gamma+1}}_{C([\theta_1,\theta_2];H^{-1}(\Omega))} \|y\|^{\frac{1}{2\gamma+1}}_{C([\theta_1,\theta_2];H^{2\gamma}(\Omega))} \\ &\le C_M^{\frac{2\gamma}{\gamma+1}} \left(\frac{C_\gamma M}{\theta_1^\gamma}\right)^{\frac{1}{2\gamma+1}} \|y\|^{\frac{2\gamma}{2\gamma+1}}_{L^2(\omega\times(\tau,T))}, \end{aligned}$$

which completes the proof of (2.3).

Step 2: logarithmic convexity. We next show an important logarithmic convexity inequality (cf. [1] [9]) for our inverse problem:

$$\|y(\cdot,t)\|_{L^2(\Omega)} \le \|y(\cdot,0)\|^{1-\frac{t}{\theta}}_{L^2(\Omega)} \|y(\cdot,\theta)\|^{\frac{t}{\theta}}_{L^2(\Omega)} \quad \text{for all } 0 \le t \le \theta, \tag{2.10}$$

which will then lead to the following estimate:

$$\|y\|_{L^2(0,\theta;L^2(\Omega))} \le C_M\Big(-\log \|y\|_{L^2(\omega\times(\tau,T))}\Big)^{-1/2}. \tag{2.11}$$

Let us first prove (2.10). For this, we consider the function

$$V(t) = \|y(\cdot,t)\|^2_{L^2(\Omega)}.$$

Using (1.1) and the integration by parts we can easily see that

$$\begin{aligned} V'(t) &= 2\int_\Omega y(x,t)\, y_t(x,t)dx = 2\int_\Omega y(x,t)\,(A\,y)(x,t)dx \\ &= -2\int_\Omega \sum_{i,j=1}^n a_{ij}\frac{\partial y}{\partial x_i}\frac{\partial y}{\partial x_j}\,dx - 2\int_\Omega c(x)\,y^2\,dx\,. \end{aligned}$$

Further differentiating and integrating by parts, we have

$$V''(t) = -4\int_\Omega \Big[\sum_{i,j=1}^n a_{ij}\frac{\partial y}{\partial x_j}\frac{\partial^2 y}{\partial x_i \partial t}dx + c(x) y y_t\Big]dx = 4\int_\Omega y_t\,Ay\,dx = 4\int_\Omega y_t(x,t)^2 dx.$$

Using the above formulae for $V'(t)$ and $V''(t)$ and the Cauchy-Schwarz inequality, we have

$$V'(t)^2 - V''(t)V(t) = \Big(2\int_\Omega y y_t dx\Big)^2 - 4\int_\Omega {y_t}^2 dx \int_\Omega y^2 dx \le 0,$$

this yields

$$(\log V(t))'' = \frac{V''(t)V(t) - V'(t)^2}{V(t)^2} \ge 0.$$

Therefore we know that $\log V(t)$ is convex, which leads to

$$\log V(t) \le (1-\frac{t}{\theta})\log V(0) + \frac{t}{\theta}\log V(\theta),$$

or

$$V(t) \leq V(0)^{1-\frac{t}{\theta}} V(\theta)^{\frac{t}{\theta}},$$

which gives (2.10).

To show (2.11), we square both sides of (2.10) and then integrate over $t \in (0, \theta)$ to obtain

$$\int_0^\theta \|y(\cdot,t)\|^2_{L^2(\Omega)} dt \leq C_M \int_0^\theta \|y(\cdot,\theta)\|^{\frac{2t}{\theta}}_{L^2(\Omega)}\, dt\,. \tag{2.12}$$

Now by a slight manipulation and using (2.3), we get

$$\|y\|_{L^2(0,\theta;L^2(\Omega))} \leq C_M \Big(-\log \|y(\cdot,\theta)\|_{L^2(\Omega)} \Big)^{-\frac{1}{2}} \leq C_M \Big(-\log \|y\|_{L^2(\omega\times(\tau,T))} \Big)^{-\frac{1}{2}},$$

which proves (2.11).

Step 3: the desired stability estimate. By the semigroup representation of the solution $y(x,t)$, we can easily see

$$y_t(\cdot,t) = A\, e^{tA} y(\cdot,0) = -(-A)^{1-\varepsilon} e^{tA} (-A)^{\varepsilon} y(\cdot,0),$$

then using (2.8) we obtain

$$\|y_t(\cdot,t)\|_{L^2(\Omega)} \leq C\, t^{\varepsilon-1} \|(-A)^\varepsilon y(\cdot,0)\|_{L^2(\Omega)}.$$

Now for any $1 < p < 1/(1-\varepsilon)$, noting $y(\cdot,0) \in \mathcal{A}$, we obtain that

$$\int_0^\theta \|y_t(\cdot,t)\|^p_{L^2(\Omega)} dt \leq C \int_0^\theta t^{p(\varepsilon-1)} dt\, \|(-A)^\varepsilon y(\cdot,0)\|^p_{L^2(\Omega)} \leq C \|y(\cdot,0)\|^p_{H^{2\varepsilon}(\Omega)} \leq C(M).$$

This proves

$$\|y\|_{W^{1,p}(0,\theta;L^2(\Omega))} \leq C(M). \tag{2.13}$$

We note that we can choose p such that $1 < p \leq 2$. On the other hand, by (2.11) and the fact that $\|\eta\|_{L^p(0,T)} \leq C\|\eta\|_{L^2(0,T)}$ for $p \leq 2$ we have

$$\|y\|_{L^p(0,\theta;L^2(\Omega))} \leq C(M) \Big(-\log \|y\|_{L^2(\omega\times(\tau,T))} \Big)^{-\frac{1}{2}}. \tag{2.14}$$

Using (2.13), (2.14) and the Sobolev interpolation, we derive for $0 < s < 1$ that

$$\|y\|_{W^{1-s,p}(0,\theta;L^2(\Omega))} \leq C(M) \Big(-\log \|y\|_{L^2(\omega\times(\tau,T))} \Big)^{-\frac{s}{2}}. \tag{2.15}$$

Now one may choose $s \in (0,1)$ such that $(1-s)p > 1$ and space $W^{1-s,p}(0,\theta;L^2(\Omega))$ can be continuously embedded into $C([0,\theta];L^2(\Omega))$, and we then derive from (2.15) that

$$\|y\|_{C([0,\theta];L^2(\Omega))} \leq \|y\|_{W^{1-s,p}(0,\theta;L^2(\Omega))} \leq C(M) \Big(-\log \|y\|_{L^2(\omega\times(\tau,T))} \Big)^{-\frac{s}{2}}.$$

This completes the proof of the theorem. □

To establish a similar conditional stability estimate for **Inverse Problem II** with the boundary measurement data of heat flux $\partial_\nu y$ on $\Gamma \times (\tau, T)$, the following technical lemma (see Theorem 2.1 in Yuan and Yamamoto [20]) is crucial:

Lemma 2.1. *Let β be a given positive constant and θ be fixed such that $0 < \tau < \theta < T$. Let $\varphi(x,t) = \exp(\lambda(d(x) - \beta|t-\theta|^2))$, with function d to be determined.*

Then there exist a non-negative function $d \in C^2(\bar{\Omega})$ and a number $\lambda_0 > 0$ such that for each $\lambda \geq \lambda_0$, one can choose a constant $s_0(\lambda) \geq 0$ so that the estimate

$$\begin{aligned}&\int_{\Omega\times(\tau,T)} \left\{ \frac{1}{s}\left(\left|\frac{\partial v}{\partial t}\right|^2 + \sum_{i,j=1}^{n} \left|\frac{\partial^2 v}{\partial x_i \partial x_j}\right|^2 \right) + s|\nabla v|^2 + s^3|v|^2 \right\} e^{2s\varphi} dxdt \\ \leq &C_1 \int_{\Omega\times(\tau,T)} |(\partial_t - A)v|^2 e^{2s\varphi} dxdt + C_1 s \int_\tau^T \int_\Gamma |\partial_\nu v|^2 e^{2s\varphi} d\Sigma\end{aligned} \tag{2.16}$$

holds for some constant $C_1 = C_1(s_0, \lambda) > 0$ and all $s \geq s_0$ and all v satisfying that $v(\cdot,\tau) = v(\cdot,T) = 0$ and

$$v \in L^2(\tau, T; H^2(\Omega) \cap H_0^1(\Omega)), \quad (\partial_t - A)v \in L^2(\Omega \times (\tau, T)).$$

With the preparations above, we can now state our second main theorem of this section:

Theorem 2.2. *Let $\Gamma \subset \partial\Omega$ be an arbitrary relatively open subset of $\partial\Omega$, and $y(x,t)$ be the solution to (1.1). For any $y(\cdot,0) \in \mathcal{A}$, there exists a constant $\kappa = \kappa(M,\varepsilon) \in (0,1)$ such that*

$$\|y(\cdot,0)\|_{L^2(\Omega)} \leq C(M,\varepsilon)(-\log \|\partial_\nu y\|_{L^2(\Gamma\times(\tau,T))})^{-\kappa}.$$

Proof. It suffices to prove that for any $\theta \in (\tau, T)$ there exist constants $C(M)$ and $\kappa_1 \in (0,1)$ such that

$$\|y(\cdot,\theta)\|_{L^2(\Omega)} \leq C(M)\|\partial_\nu y\|^{\kappa_1}_{L^2(\Gamma\times(\tau,T))}. \tag{2.17}$$

With the estimate (2.17) and the Carleman estimate in Lemma 2.1, the proof of Theorem 2.2 can be shown by following Steps 2 and 3 of the proof of Theorem 2.1.

We choose $\beta > 0$ such that

$$\sup_{x\in\Omega} d(x) < \beta \min\{|\tau-\theta|^2, |T-\theta|^2\},$$

and set $d_0 = \inf_{x\in\Omega} \exp\{\lambda d(x)\} \geq 1$. Then by the choice of $\beta > 0$, we can check that

$$\varphi(x,\theta) \geq d_0, \quad \varphi(x,\tau), \varphi(x,T) < 1 \leq d_0, \quad \forall\, x \in \overline{\Omega}.$$

Thus for a sufficiently small $\varepsilon_1 > 0$, we can choose a small $\varepsilon_2 = \varepsilon_2(\varepsilon_1) > 0$ such that $\tau < \tau + 2\varepsilon_2 < \theta - \varepsilon_2 < \theta + \varepsilon_2 < T - 2\varepsilon_2 < T$, and

$$\varphi(x,t) \geq d_0 - \varepsilon_1, \quad \forall\,(x,t) \in \overline{\Omega} \times [\theta-\varepsilon_2, \theta+\varepsilon_2]; \tag{2.18}$$

$$\varphi(x,t) \leq d_0 - 2\varepsilon_1, \quad \forall\,(x,t) \in \overline{\Omega} \times ([\tau, \tau+2\varepsilon_2] \cup [T-2\varepsilon_2, T]). \tag{2.19}$$

Now we introduce a cut-off function $\chi \in C_0^\infty(0,T)$ such that $0 \leq \chi \leq 1$, and

$$\chi(t) = \begin{cases} 0, & t \in [\tau, \tau+\varepsilon_2] \cup [T-\varepsilon_2, T]; \\ 1, & t \in [\tau+2\varepsilon_2, T-2\varepsilon_2]. \end{cases} \tag{2.20}$$

Consider the function $v = \chi\, y$, and one can easily verify that $(\partial_t - A)v = (\partial_t\chi)y$ in $\Omega \times (\tau, T)$. Then we can apply Lemma 2.1 to this v to derive

$$\begin{aligned}&\int_{\Omega\times(\tau,T)} \left(\frac{1}{s}|\partial_t v|^2 + s^3|v|^2\right) e^{2s\varphi} dxdt \\ \leq &C_1 \int_{\Omega\times(\tau,T)} |\partial_t \chi|^2 |y|^2 e^{2s\varphi} dxdt + C_1 s \int_\tau^T \int_\Gamma |\partial_\nu v|^2 e^{2s\varphi} d\Sigma\end{aligned} \tag{2.21}$$

for all $s \geq s_0$. By (2.19) and (2.20), we obtain from (2.21) that

$$\begin{aligned}\int_{\Omega\times(\tau,T)} |\partial_t\chi|^2|y|^2e^{2s\varphi}dxdt &= \left(\int_{\tau+\varepsilon_2}^{\tau+2\varepsilon_2}\int_\Omega + \int_{T-2\varepsilon_2}^{T-\varepsilon_2}\int_\Omega\right)|\partial_t\chi|^2|y|^2e^{2s\varphi}dxdt \\ &\leq e^{2s(d_0-2\varepsilon_1)}\left(\int_{\tau+\varepsilon_2}^{\tau+2\varepsilon_2}\int_\Omega + \int_{T-2\varepsilon_2}^{T-\varepsilon_2}\int_\Omega\right)|\partial_t\chi|^2|y|^2dxdt \\ &\leq C_1e^{2s(d_0-2\varepsilon_1)}\|y\|^2_{L^2(\Omega\times(\tau,T))}.\end{aligned}$$

Using this estimate and (2.18), we have

$$\begin{aligned}&e^{2s(d_0-\varepsilon_1)}\int_\Omega\int_{\theta-\varepsilon_2}^{\theta+\varepsilon_2}\left(\frac{1}{s}|\partial_t y|^2 + s^3|y|^2\right)dxdt \\ \leq &\int_\Omega\int_{\theta-\varepsilon_2}^{\theta+\varepsilon_2}\left(\frac{1}{s}|\partial_t v|^2 + s^3|v|^2\right)e^{2s\varphi}dxdt \\ \leq &C_1e^{2s(d_0-2\varepsilon_1)}\|y\|^2_{L^2(\Omega\times(\tau,T))} + C_1se^{2s\Phi}\|\partial_\nu y\|^2_{L^2(\Gamma\times(\tau,T))},\end{aligned}$$

with $\Phi = \sup_{(x,t)\in\Gamma\times(\tau,T)}\varphi(x,t)$. This implies immediately that

$$\begin{aligned}&\frac{e^{2s(d_0-\varepsilon_1)}}{s}\|y\|^2_{H^1(\theta-\varepsilon_2,\theta+\varepsilon_2;L^2(\Omega))} \\ \leq &C_1e^{2s(d_0-2\varepsilon_1)}\|y\|^2_{L^2(\Omega\times(\tau,T))} + C_1se^{2s\Phi}\|\partial_\nu y\|^2_{L^2(\Gamma\times(\tau,T))}\end{aligned}$$

for all $s \geq s_0$. Then by the Sobolev embedding theorem, we derive

$$\begin{aligned}C_3^{-1}\|y(\cdot,\theta)\|^2_{L^2(\Omega)} &\leq \|y\|^2_{H^1(\theta-\varepsilon_2,\theta+\varepsilon_2;L^2(\Omega))} \\ &\leq sC_1e^{-2s\varepsilon_1}\|y\|^2_{L^2(\Omega\times(\tau,T))} + C_2e^{C_2s}\|\partial_\nu y\|^2_{L^2(\Gamma\times(\tau,T))}. \qquad (2.22)\end{aligned}$$

But noting that $a \in \mathcal{A}$, we have by the semigroup theory (see, e.g., [11]) that

$$\|y\|^2_{L^2(\Omega\times(\tau,T))} \leq \int_\tau^T \|e^{At}a\|^2_{L^2(\Omega)}dt \leq M^2C_4(T)\,,$$

where $C_4(T) > 0$ does not depend on the special choice of a in $\mathcal{A}$. Hence we obtain from (2.22) that

$$\|y(\cdot,\theta)\|^2_{L^2(\Omega)} \leq C_1M^2C_4(T)se^{-2s\varepsilon_1} + C_2e^{C_2s}\|\partial_\nu y\|^2_{L^2(\Gamma\times(\tau,T))}$$

for all $s \geq s_0$. By shifting the variable s, we can easily see

$$\begin{aligned}\|y(\cdot,\theta)\|^2_{L^2(\Omega)} &\leq C_1M^2C_4(T)(s+s_0)e^{-2(s+s_0)\varepsilon_1} + C_2e^{C_2(s+s_0)}\|\partial_\nu y\|^2_{L^2(\Gamma\times(\tau,T))} \\ &\leq M^2C_5(\varepsilon_1,T)e^{-s\varepsilon_1} + C_6e^{C_6s}\|\partial_\nu y\|^2_{L^2(\Gamma\times(\tau,T))}\end{aligned}$$

for all $s \geq 0$. Here we have used the fact that $\eta e^{-\eta\varepsilon_1} \leq 1/\varepsilon_1$ for all $\eta \geq 0$ and dropped the dependence on s_0.

Next we consider two cases. For $\frac{M}{\|\partial_\nu y\|_{L^2(\Gamma\times(\tau,T))}} > 1$, we set

$$s = \frac{2}{C_6+\varepsilon_1}\log\frac{M}{\|\partial_\nu y\|_{L^2(\Gamma\times(\tau,T))}},$$

then we obtain

$$\|y(\cdot,\theta)\|^2_{L^2(\Omega)} \leq (C_6 + C_5(\varepsilon_1,T))\,M^{\frac{2C_6}{C_6+\varepsilon_1}}\|\partial_\nu y\|^{\frac{2\varepsilon_1}{C_6+\varepsilon_1}}_{L^2(\Gamma\times(\tau,T))}\,,$$

which clearly implies (2.17) with $\kappa_1 = \frac{\varepsilon_1}{C_6+\varepsilon_1}$.

For $\frac{M}{\|\partial_\nu y\|_{L^2(\Gamma\times(\tau,T))}} \le 1$, we can apply the semigroup theory (e.g., [11]) by noting that $a \in \mathcal{A}$ to get $\|y(\cdot,\theta)\|_{L^2(\Omega)} \le C_8(M)$ and

$$\|\partial_\nu y\|_{L^2(\Gamma\times(\tau,T))} \le C_7\|y\|_{L^2(\tau,T;H^2(\Omega))} \le C_8(M).$$

Therefore we derive

$$\begin{aligned} \|y(\cdot,\theta)\|^2_{L^2(\Omega)} &\le C_8(M) \le \frac{C_8(M)}{M}\|\partial_\nu y\|_{L^2(\Gamma\times(\tau,T))} \\ &\le \frac{C_8(M)}{M}C_8(M)^{1-\kappa_1}\|\partial_\nu y\|^{\kappa_1}_{L^2(\Gamma\times(\tau,T))}, \end{aligned} \tag{2.23}$$

which proves (2.17). □

Before we start the numerical experiments, we make a few remarks on some existing theoretical results that may be related somehow to ours in this section.

Remark 2.2. We refer to Lees and Protter [9], Lavrent'ev, Romanov and Shishat·skii [8](section 2 of Chapter IV) for some early work which uses the Carleman-type estimates as effective tools to establish conditional stability estimates for the backward heat conduction problem.

Remark 2.3. There are some results, related to ours in Theorem 2.1, in the literature, see, e.g., Klibanov [6], Saitoh and Yamamoto [14], Xu and Yamamoto [16]. Very restrictive requirements and smoothness are assumed on the measurement data in [14] so that all the derivatives of the initial data can be recovered. In [16], the measurement data of $\nabla y(x,t)$ or $y(x,t)$ were assumed to be available in a small subregion ω but for all the times in the interval $(0,T)$. A conditional stability estimate was established in [6] for a general parabolic equation $y_t = A(x,t)y$ by using the lateral Cauchy data for all the times in the interval $[0,T]$, where the coefficients in the heat equation depend both on x and t, and the elliptic operator $A(x,t)$ is second order and not necessarily symmetric. Moreover, the stability in [6] holds also for a parabolic inequality, and can be applied to a numerical method similar to the quasi-reversibilty. Furthermore, the index κ in (2.2) is allowed to be 1 in [6], but more smoothness for the unknown initial values is necessary , i.e., it requires $\varepsilon = 1/2$ in (2.1).

3. **Numerical reconstruction method.** In this section, we shall study the numerical reconstruction of the initial temperature by means of some observation data of temperature, which leads to a stable reconstruction based on the stability theory established in the previous section. Without loss of generality, we shall consider the following model problem and recover the initial temperature profile $\mu(x)$ in the whole domain Ω:

$$\begin{aligned} \frac{\partial y}{\partial t} &= \Delta y(x,t) + f(x,t)\,, && (x,t)\in\Omega\times(0,T), \\ y(x,0) &= \mu(x)\,, && x\in\Omega, \\ y(x,t) &= \eta_1(x)\,, && (x,t)\in\Gamma_D\times(0,T), \\ \frac{\partial y}{\partial n}(x,t) &= \eta_2(x)\,, && (x,t)\in\Gamma_N\times(0,T), \end{aligned} \tag{3.1}$$

where Ω is a bounded and connected one-dimensional line segment or two-dimensional polygonal domain and $\partial\Omega = \Gamma_D \cup \Gamma_N$. The observed data will be taken to be

$$\nabla z(x,t) = \nabla y(x,t) \quad \text{or} \quad z(x,t) = y(x,t), \quad (x,t)\in\omega\times(\tau,T)$$

for some fixed $\tau > 0$, and we shall call them the H^1-data case and L^2-data case, respectively. For the boundary measurement case, we will take the flux measurement data, namely $\partial_n z = \partial_n y$.

We will first derive the continuous formulation of the problem and its finite element approximation, and then present the convergence of the finite element solution and its numerical experiments.

3.1. **The continuous formulation.** The conditional stability established in Section 2 provides us with some important guidance for the possible numerical reconstruction. With a priori knowledge of the boundedness of the initial temperature and appropriate observation data, it is possible for us to reconstruct the initial temperature profile through the classical Tikhonov regularization technique. In this work we shall confine ourself to the case when $\varepsilon = 1/2$ in (2.1), in which case the initial temperature profile lies in the function space $H^1(\Omega)$. The analysis for the general case is much more complicated and will be left for some future study.

We formulate the reconstruction of the initial temperature μ in (3.1) as the following constrained minimization problem:

$$\min_{\mu\in K_1} \ J(\mu) = \frac{1}{2}\int_\tau^T \int_\omega (y(\mu) - z)^2 \ \mathrm{d}x\mathrm{d}t + \gamma \int_\Omega |\nabla\mu|^2 \ \mathrm{d}x \tag{3.2}$$

when the L^2-data are available, and

$$\min_{\mu\in K_2} \ J(\mu) = \frac{1}{2}\int_\tau^T \int_\omega |\nabla y(\mu) - \nabla z|^2 \ \mathrm{d}x\mathrm{d}t + \gamma \int_\Omega |\nabla\mu|^2 \ \mathrm{d}x \tag{3.3}$$

when the H^1-data are available. Here we denote by γ the regularization parameter and the constraint sets K_i $(i = 1, 2)$ above are chosen to be

$$K_i = \{\mu \in H^1(\Omega);\ |\mu(x)| \le \alpha_i \text{ in } \Omega\},$$

where α_1 and α_2 are two positive constants.

The solutions $y = y(\mu)$ in (3.2) and (3.3) satisfy the variational formulation associated with the parabolic system (3.1):

$$y(x, 0) = \mu(x) \quad \text{in } \Omega; \qquad y(x, t) = \eta_1(x, t) \quad \text{on } \Gamma_D \times (0, T) \tag{3.4}$$

$$\int_\Omega y_t\phi \ \mathrm{d}x + \int_\Omega \nabla y \cdot \nabla\phi \ \mathrm{d}x = \int_\Omega f\phi \ \mathrm{d}x + \int_{\Gamma_N} \eta_2\phi \ \mathrm{d}s \quad \forall\, \phi \in H^1_{\Gamma_D}(\Omega) \tag{3.5}$$

for a.e. $t \in (0, T)$, where $H^1_{\Gamma_D}(\Omega)$ is a subspace of $H^1(\Omega)$ with all functions vanishing on Γ_D.

For the minimization problems (3.2) and (3.3), we can show

Theorem 3.1. *There exists at least a minimizer to the minimization problems (3.2) and (3.3), respectively.*

Proof. We give only an outline of the proof for the minimization problem (3.2), and the proof is basically the same for (3.3).

First of all, due to the non-negativeness of the cost functional $J(\mu)$, one can easily see that $J(\mu)$ is bounded from below over the constraint set K_1, which implies that there exists a minimizing sequence $\{\mu_m\}$ in K_1 such that

$$\lim_{m\to\infty} J(\mu_m) = \inf_{\mu\in K_1} J(\mu).$$

Thanks to the boundedness of this minimizing sequence $\{\mu_m\}$ in $H^1(\Omega)$, we can extract a subsequence, still denoted by $\{\mu_m\}$, such that μ_m converges weakly to μ^* in $H^1(\Omega)$.

Now applying a duality argument for parabolic systems, similarly to that done in [5, Lemma 2.1], we can conclude that $y(\mu_m)$ converges weakly to $y(\mu^*)$ in $L^2(0,T;H^1(\Omega))$, and more,

$$\lim_{m\to\infty}\int_\tau^T\int_\omega |(y(\mu_m)-z)|^2 \,\mathrm{d}x\mathrm{d}t = \int_\tau^T\int_\omega |(y(\mu^*)-z)|^2 \,\mathrm{d}x\mathrm{d}t.$$

Then the weakly lower semicontinuity of $J(\mu)$ ensures that μ^* is a minimizer, which completes the proof. □

3.2. **Finite element discretization and its convergence.** In this subsection, the finite element discretization scheme will be proposed for solving the continuous minimization problems (3.2) and (3.3). We will focus on the formulation (3.2) for its finite element discretization and convergence, while one can do in parallel for the formulation (3.3), only with some minor modifications.

First we triangulate the domain Ω with a shape regular triangulation $\mathcal{T}^h$ of simplicial elements, and define V_h to be the continuous piecewise linear finite element space defined over $\mathcal{T}^h$ and $\overset{\circ}{V}_h$ a subspace of V_h with all functions vanishing on the boundary Γ_D. For the time discretization, we divide the time interval $(0,T)$ into M equally-spaced subintervals by using nodal points

$$0=t^0<t^1<\cdots<t^M=T$$

with $t^n = n\Delta t,\ \Delta t = T/M$. Assume that the starting observation time τ is taken such that $\tau = n_0\Delta t$ for some integer $n_0>0$. For a continuous mapping $y:[0,T]\to L^2(\Omega)$, we define $y^n = y(\cdot, n\Delta t)$ for $0\le n\le M$. For a given sequence $\{y^n\}_{n=0}^M \subset L^2(\Omega)$ we define the difference quotient and the averaging function

$$\partial_{\Delta t}y^n = \frac{y^n-y^{n-1}}{\Delta t}, \qquad \bar{y}^n = \frac{1}{\Delta t}\int_{t^{n-1}}^{t^n} y(t)\,dt\,. \tag{3.6}$$

With the notations above and the discrtization of the first term of (3.2) by the composite trapezoidal rule in time, we can formulate the finite element approximation of the problem (3.2) as follows:

$$\min_{\mu_h\in V_h\cap K_1} J_h(\mu_h) = \frac{\Delta t}{2}\sum_{n=0}^M c_n\int_\omega |(y_h^n(\mu_h)-z^n)|^2 \,\mathrm{d}x + \gamma\int_\Omega |\nabla\mu_h|^2 \,\mathrm{d}x \tag{3.7}$$

where $y_h^n \equiv y_h^n(\mu_h)\in V_h$ for $n=0,1,\cdots,M$ satisfies

$$y_h^0 = \mu_h \quad \text{ and } \quad y_h^n = Q_h\bar{\eta}_1^n + \hat{y}_h^n, \tag{3.8}$$

$$\int_\Omega \partial_{\Delta t}y_h^n\phi_h \,\mathrm{d}x + \int_\Omega \nabla y_h^n\cdot\nabla\phi_h \,\mathrm{d}x = \int_\Omega f\,\phi_h \,\mathrm{d}x + \int_{\Gamma_N}\eta_2\phi_h \,\mathrm{d}s \tag{3.9}$$

for all $\phi_h \in \overset{\circ}{V}_h$. Here $c_{n_0} = c_M = 1/2$, $c_n = 1$ for $n_0<n<M$, $c_n = 0$ otherwise. $Q_h\bar{\eta}_1^n$ is the interpolation or L^2-projection of $\bar{\eta}_1^n$ in V_h, and $\hat{y}_h^n \in \overset{\circ}{V}_h$ (cf. [15]).

The following theorem addresses the existence of the minimizers to the discrete minimization problem (3.7)-(3.9), whose proof basically follows the same lines as that in [5, Theorem 3.1].

Theorem 3.2. *There exists at least a minimizer to the discrete minimization problem (3.7)-(3.9).*

The following technical lemma is crucial to the demonstration of the convergence of the finite element solution, and the proof can be done by following that of [18, Lemma 4.4].

Lemma 3.3. *For any sequence $\{\mu_h\}_{h>0}$ in V_h, which converges to μ in $H^1(\Omega)$ as $h \to 0$, it holds*

$$\frac{\Delta t}{2}\sum_{n=n_0}^{M} c_n \int_\omega |(y_h^n(\mu_h) - z^n)|^2 \ dx \to \int_\tau^T \int_\omega |(y(\mu) - z)|^2 \ dx dt$$

when $h \to 0$ and $\Delta t \to 0$.

Now we are in a position to show the convergence of the finite element solution to the discrete system (3.7)-(3.9).

Theorem 3.4. *Let $\{\mu_h^*\}_{h>0}$ be a sequence of minimizers of the discrete minimization problem (3.7)-(3.9). Then each subsequence of $\{\mu_h^*\}_{h>0}$ has a subsequence converging in $L^2(\Omega)$ to a minimizer of the continuous problem* (3.2)*. If the minimizer of the continuous problem is unique, then the whole sequence $\{\mu_h^*\}_{h>0}$ converges to the unique minimizer of* (3.2).

Proof. It is easy to verify that $J_h(\mu_h^*) \le C$ for some constant C independent of the meshsize h and time step Δt, which implies the boundedness of $\{\mu_h^*\}_{h>0}$ in $H^1(\Omega)$. Hence one can extract a subsequence of μ_h^*, still denoted as $\{\mu_h^*\}$, such that

$$\mu_h^* \to \mu^* \quad \text{weakly in } H^1(\Omega).$$

Then for any $\mu \in K_1$, the weak lower semicontinuity and the stability properties of a quasi-L^2 projection operator $\pi_h : L^2(\Omega) \to V_h$ (cf. [17]) combined with Lemma 3.3 yield

$$\begin{aligned}
J(\mu^*) &\le \lim_{\substack{h\to 0\\ \Delta t \to 0}} \frac{\Delta t}{2}\sum_{n=n_0}^{M} c_n \int_\omega |(y_h^n(\mu_h^*) - z^n)|^2 \ \mathrm{d}x + \gamma \liminf_{\substack{h\to 0\\ \Delta t \to 0}} \int_\Omega |\nabla \mu_h^*|^2 \ \mathrm{d}x \\
&\le \liminf_{\substack{h\to 0\\ \Delta t \to 0}} J_h(\mu_h^*) \le \liminf_{\substack{h\to 0\\ \Delta t \to 0}} J_h(\pi_h \mu) \\
&= \frac{1}{2}\int_\tau^T \int_\omega |y(\mu) - z|^2 \ \mathrm{d}x\mathrm{d}t + \gamma \int_\Omega |\nabla \mu|^2 \ \mathrm{d}x \\
&= J(\mu).
\end{aligned}$$

This implies that μ^* is indeed a minimizer of the continuous minimization problem (3.3). The rest of the proof is quite standard. $\square$

3.3. **Numerical algorithm.** In this subsection, we present a numerical reconstruction algorithm for solving the discretized finite element minimization problem (3.7)-(3.9). For the purpose we need to calculate the Gateaux derivative $J_h'(\mu_h)\lambda_h$ of $J_h(\mu_h)$ at any given direction $\lambda_h \in V_h$.

First of all, we note that the Gateaux derivative for the discrete parabolic solution $y_h^n(\mu_h)$ at any given direction $\lambda_h \in V_h$, denoted as $(y_h^n)'(\mu_h)\lambda_h$, solves the following discrete system: $\xi_h^0 = \lambda_h$ and $\xi_h^n \equiv (y_h^n)'(\mu_h)\lambda_h \in V_h^0$ for $n = 1, 2, \ldots$, satisfies

$$\int_\Omega \partial_{\Delta t}\xi_h^n \phi_h \ \mathrm{d}x + \int_\Omega \nabla \xi_h^n \cdot \nabla \phi_h \ \mathrm{d}x = 0\,, \quad \forall\, \phi_h \in \mathring{V}_h\,. \tag{3.10}$$

For the ease of computing the derivative $J_h'(\mu_h)\lambda_h$ along each individual direction, we introduce a discrete sequence $\{w_h^n\}_{n=0}^M \subset \mathring{V}_h$ such that $w_h^M = 0$ and $w_h^n \in \mathring{V}_h$ for $0 \le n < M$ solves the discrete backward parabolic equation

$$-\int_\Omega \partial_{\Delta t} w_h^n \phi_h \, \mathrm{d}x + \int_\Omega \nabla w_h^{n-1} \cdot \nabla \phi_h \, \mathrm{d}x = \Delta t \, c_n \int_\omega (y_h^n(\mu_h) - z^n)\phi_h \, \mathrm{d}x. \quad (3.11)$$

Using (3.10) and (3.11), we come to the following simple formula for evaluating $J_h'(\mu_h)\lambda_h$:

$$J_h'(\mu_h)\lambda_h = \frac{1}{\tau}\int_\Omega w_h^0 \lambda_h \, \mathrm{d}x + 2\gamma \int_\Omega \nabla \mu_h \cdot \nabla \lambda_h \, \mathrm{d}x \,. \quad (3.12)$$

With the formula (3.12) we can now present the following reconstruction algorithm for solving the discrete minimization problem (3.7)–(3.9).

Reconstruction algorithm :

1. Choose an initial value $\mu_h^{(0)} \in V_h$ and set $k = 0$.
2. Compute $\{y_h^n\}_{n=0}^M$ from the discrete parabolic problem (3.8)–(3.9) using $\mu_h^{(k)}$.
3. Compute the adjoint state $\{w_h^n\}_{n=0}^M$ from the adjoint problem (3.11) using $\{y_h^n\}_{n=0}^M$.
4. Evaluate the components of $J_h'(\mu_h)$ corresponding to all basis functions ϕ_i from V_h:
$$g_i = \frac{1}{\tau}\int_\Omega w_h^0 \phi_i \, \mathrm{d}x + 2\gamma \int_\Omega \nabla \mu_h^{(k)} \cdot \nabla \phi_i \, \mathrm{d}x.$$
Set $g_h = \sum_i g_i \phi_i$.
5. Find some $s > 0$ such that $J_h(\mu_h^{(k)} - s g_h) < J_h(\mu_h^{(k)})$ using the inexact line search.
6. If $\|\mu_h^{(k+1)} - \mu_h^{(k)}\| \le$ tolerance, or the number of iterations is greater than some prescribed value, stop; otherwise, set $k := k + 1$ and goto Step 2.

Remark 3.1. In the previous reconstruction algorithm, one can achieve a Gateaux derivative along all directions by solving a backward parabolic system once at each iteration. For practical issues like the construction of some fast solvers to accelerate the numerical reconstruction process, we refer readers to our earlier work [10, 18].

Remark 3.2. When the observable subdomain ω lies on part of the boundary of the considered domain, the finite element spaces V_h and $\mathring{V}_h$ should be modified accordingly. And the first integral in the right-hand side of (3.7) is an integral along some boundary part. The derivation of the Gateaux derivative can be carried out in a similar manner.

4. **Numerical experiments.** For the one-dimensional case, we take $\Omega = (0, 1)$, $T = 1$; and Ω is partitioned by a finite element grid of mesh size $h = 1/80$. For the two-dimensional case, we take $\Omega = (0, 1)\times(0, 1)$, $T = 1$; and the finite element mesh on Ω of mesh size $h = 1/32$ is formed by dividing Ω into 32×32 equal sub-squares and then partitioning each sub-square through its diagonal into two triangles. The time step size $\Delta t = 1/1000$. The observed data are only available on a subdomain ω of Ω or on a relatively open subset Γ_0 of the boundary $\partial\Omega$. Without loss of generality, the initially guessed temperature profile $\mu_h^{(0)}$ is always taken to be zero everywhere in the domain Ω.

In all our numerical simulations, we assume that the observation data have certain observation errors of random distribution. Instead of using the exact data y or ∇y, we take the noisy data of the following form:

$$z(x,t) = y(x,t)(1 + \delta R(x,t)) \quad \text{or} \quad \nabla z(x,t) = \nabla y(x,t)(1 + \delta R(x,t))$$

for the one-dimensional examples, and

$$z(x,y,t) = y(x,y,t)(1 + \delta R(x,y,t)) \quad \text{or} \quad \nabla z(x,y,t) = \nabla y(x,y,t)(1 + \delta R(x,y,t))$$

for the two-dimensional examples. Here $R(x,t)$ or $R(x,y,t)$ denotes a uniform random function varying in the range $[-1,1]$ and δ is the parameter representing the noise level.

Most parameters related in the proposed method are listed under each figure, including the starting observation time τ, the noise level δ, the size and position of the observation region ω, the regularization parameter γ, and the relative L^2-norm error between the exact data $\mu(x)$ and the numerically identified solution $\mu_h(x)$. The minimization problem (3.7) is solved by the reconstruction algorithm in Section 3.3 and the program halts when the following criterion is satisfied:

$$\frac{\|\mu_h^{(k+1)} - \mu_h^{(k)}\|_{L^2}}{\|\mu_h^{(k)}\|_{L^2}} \le 10^{-4}.$$

Example 1. We take the exact solution $y(x,t)$ and the initial temperature $\mu(x)$ as

$$y(x,t) = \sin(\pi x)\exp(\sin(\pi t)), \quad \mu(x) = \sin(\pi x).$$

The function $f(x,t)$ is computed through equation (3.1) using $y(x,t)$, the boundary condition $\eta_1(x,t) = 0$ on $\Gamma_D \times (0,T)$ with $\Gamma_D = \partial\Omega$ and $\Gamma_N = \emptyset$.

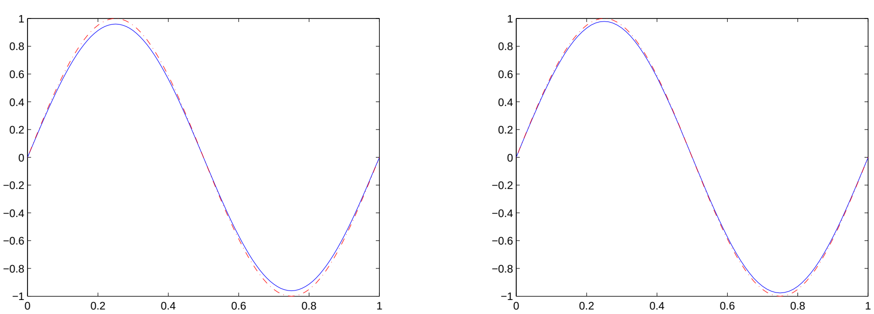

Left: $\tau = 0.1, \delta = 0.01, \gamma = 1E{-7}, iter = 5, err = 0.0395$
Right: $\tau = 0.07, \delta = 0.01, \gamma = 1E{-7}, iter = 20, err = 0.0226$

FIGURE 1. Left: reconstruction with H^1 data; Right: reconstruction with L^2 data.

Figure 1 shows the exact initial temperature $\mu(x)$ (the dashed line) and numerically reconstructed one $\mu_h(x)$ (the solid line) when the noise level $\delta = 1\%$ and the observation region $\omega = (1/5, 4/5)$ for both the H^1 and L^2 observation data. An interesting phenomenon is observed that when we increase, gradually with the step size 0.01, the starting observation time τ from 0.1 to 0.11 for the H^1 case and from 0.07 to 0.08 for the L^2 case, with all other parameters fixed, the number of iterations of the reconstruction process to achieve a good profile varies from a few to several hundreds. In the rest of the numerical examples, similar observations are obtained. To be more precise, it seems there exists a critical time $t^* > 0$. If one can measure the data in $\omega \times (\tau, T)$ with $\tau \leq t^*$, the reconstruction is relatively easy. Otherwise the reconstruction turns to be much harder when we begin the measurement after the critical time t^*.

Then we investigate the impact of the size of the observation region on the reconstruction process. Let us set the starting observation time $\tau = 0.07$ and the regularization parameter $\gamma = 1E-7$ for both observation data cases and other parameters fixed. We gradually shrink the observation region ω, which is assumed to be the central part of Ω, to find the smallest size of ω that still allows a satisfcatory reconstruction of the initial temperature in a reasonable number of iterations. Figure 2 shows the reconstruction results. It is amazing that we can recover the initial data with measurements in a quite small subregion for the H^1 data case , while for the L^2 data case one has to measure the data in a relatively larger subdomain ω. Corresponding to the critical time t^*, we find that there seems also to exist a critical size of ω. For example, with other parameters fixed, we have tried to shrink the size of ω as indicated in Figure 2 little by little and found that the reconstruction process requires more and more efforts, and finally one can only obtain extremely slow convergence until the size of ω falls below a certain value.

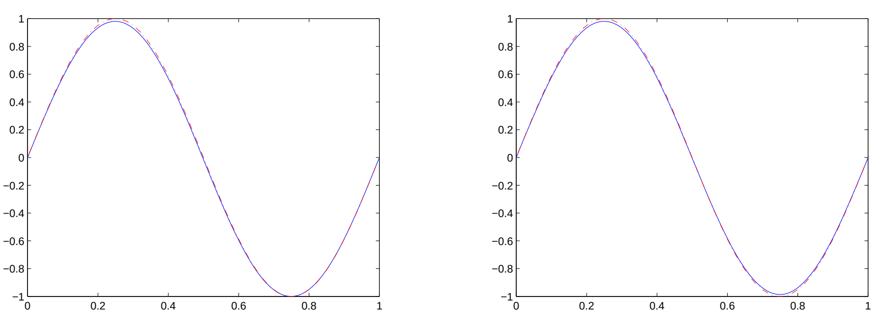

(a) $\tau = 0.07, \omega = (0.45, 0.55), iter = 3, err = 0.0169$
(b) $\tau = 0.07, \omega = (0.3, 0.7), iter = 6, err = 0.0167$

FIGURE 2. 1D initial temperature profile reconstruction in Example 1: (a) H^1-data; (b) L^2-data.

Next, we observe that there is some close relation between the starting observation time τ and the size of the observable region ω. Tables 1 and 2 present the pairs of these two parameters for the H^1-data and L^2-data cases, respectively, with other parameters fixed, which give a good profile of the initial data within a small number of iterations. From Tables 1 and 2, we see that in order to get a reasonable approximation to the initial temperature, we can either start the measurement in the early stage within a small observation region, or measure the data in a relatively large subdomain ω from a later time.

Furthermore, we have also tried to shift the observation subdomain ω gradually from left to right to study the effect on the numerical reconstruction. Figure 3 presents the exact solution $\mu(x)$ (the dashed line) and numerically reconstructed one $\mu_h(x)$ (the solid line) with different observation regions for the L^2 observation data with the noise level $\delta = 0.01$, the starting measurement time $\tau = 0.04$ and the

Starting time τ	Observation region ω	Iteration	Error
0.106	(10/80, 70/80)	5	0.0312
0.093	(20/80, 60/80)	8	0.0337
0.090	(30/80, 50/80)	7	0.0330
0.07	(36/80, 44/80)	3	0.0169
Fixed parameters: $\delta = 0.01, \gamma = 1E{-}7$.			

TABLE 1. (H^1-case) Relation between the starting observation time and the size of the observable region.

Starting time τ	Observation region ω	Iteration	Error
0.072	(10/80, 70/80)	9	0.0189
0.070	(20/80, 60/80)	9	0.0278
0.055	(30/80, 50/80)	8	0.0290
0.020	(36/80, 44/80)	10	0.0867
Fixed parameters: $\delta = 0.01, \gamma = 1E{-}9$.			

TABLE 2. (L^2-case) Relation between the starting observation time and the size of the observable region.

regularization parameter $\gamma = 1E - 7$ fixed. The reconstruction with measurement data in the central part of the domain is much faster and achieves better approximation than those with measurement data in the left or right part of the domain. When measurement data are available in the left or right part of the domain, it is interesting to notice that the numerical reconstruction is also more accurate in the left or right part of the domain accordingly, as illustrated in Figure 3 (a) and (c).

As a last testing for this example, we have tried to find out some relation between the starting time τ and the noise level δ. Figure 4 gives the maximum tolerable noise level associated with the starting observation time given with the observable region $\omega = (0.25, 0.75)$ and the regularization parameter $\gamma = 1E-7$ fixed when the L^2-data are available. From the data attached in the figure, we see that a slightly increase of the starting observing time from 0.05 to 0.06 leads to a sharp decrease of the maximum tolerable noise level from 0.12 to 0.02 for a satisfactory reconstruction of the initial data.

Remark 4.1. All the aforementioned interesting phenomena for the one-dimensional Example 1, such as the critical time and critical size of the measurement region, the effect of the position of the observation region on numerical reconstruction, as well as the relations between the starting observation time and the size of the observation region, and between the starting time and the noise level, are also observed in the subsequent one- and two-dimensional examples.

Example 2. In this example, we test a less smooth initial temperature $\mu(x)$:

$$\mu(x) = \begin{cases} x, & 0 \le x \le 1/2; \\ 1-x, & 1/2 \le x \le 1, \end{cases}$$

and the exact solution $y(x,t)$ as

$$y(x,t) = \begin{cases} \int_{-\infty}^{\infty} G(x,y,t)\mu(y)\ dy, & t > 0; \\ \mu(x), & t = 0, \end{cases}$$

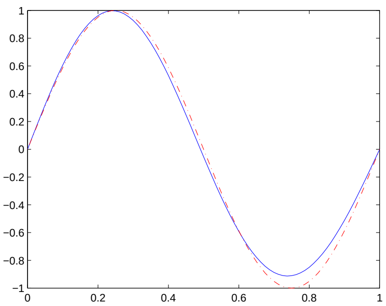

$(a)\ \omega = (1/8, 5/8), iter = 100, err = 0.074$

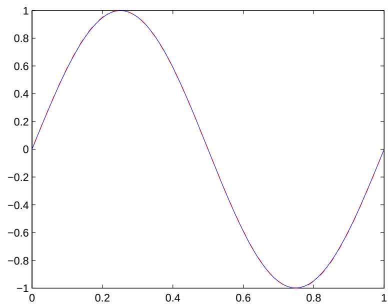

$(b)\ \omega = (1/4, 3/4), iter = 2, err = 0.0038$

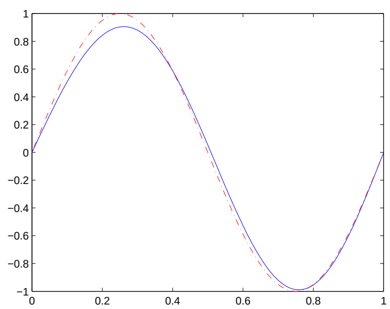

$(c)\ \omega = (3/8, 7/8), iter = 100, err = 0.0785$

FIGURE 3. Shifting observable region ω from left to right.

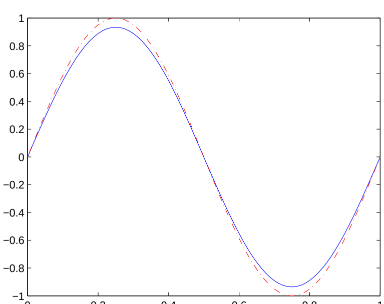

$(a)\ \tau = 0.05, \delta = 0.12, iter = 11, err = 0.065$

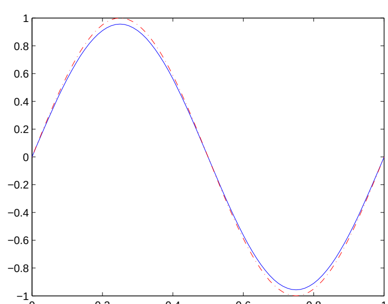

$(b)\ \tau = 0.06, \delta = 0.02, iter = 3, err = 0.0443$

FIGURE 4. Relation between the starting time and the noise level.

where

$$G(x, y, t) = \frac{1}{\sqrt{4\pi t}} \exp(-\frac{x^2}{4t})$$

is the Gaussian heat kernel. It is easy to see that $y(x, t)$ satisfies the parabolic equation (3.1) with the source term $f = 0$ and the initial data $\mu(x)$, and it has the following explicit form:

$$y(x,t) = \sqrt{\frac{t}{\pi}}\left(\exp(-\frac{(1-x)^2}{4t}) - 2\exp(-\frac{(1/2-x)^2}{4t}) + \exp(-\frac{x^2}{4t})\right) + \frac{1-x}{2}\mathrm{erf}(\frac{1-x}{2\sqrt{t}}) + \frac{2x-1}{2}\mathrm{erf}(\frac{1/2-x}{2\sqrt{t}}) - \frac{x}{2}\mathrm{erf}(\frac{-x}{2\sqrt{t}})$$

for $t > 0$, where $\mathrm{erf}(x) = \frac{2}{\pi}\int_0^x e^{-t^2}\,dt$. The boundary function is set to be $\eta_1(x,t) = y(x,t)$ on $\Gamma_D \times (0,T)$ with $\Gamma_D = \partial\Omega$ and $\Gamma_N = \emptyset$, the starting observation time $\tau = 0.01$, the L^2 measurement data are obtained by adding uniform random values, and the regularization parameter $\gamma = 1E-7$.

The difficulty of this example lies in the singular point in the initial temperature. Figure 5 shows the exact initial data $\mu(x)$ (the dashed line) and numerically reconstructed one $\mu_h(x)$ (the solid line). We note that although there is a singular point in $\mu(x)$, the finite element identified solution $\mu_h(x)$ matches very well with $\mu(x)$ except for some oversmoothed side-effect around the singular point.

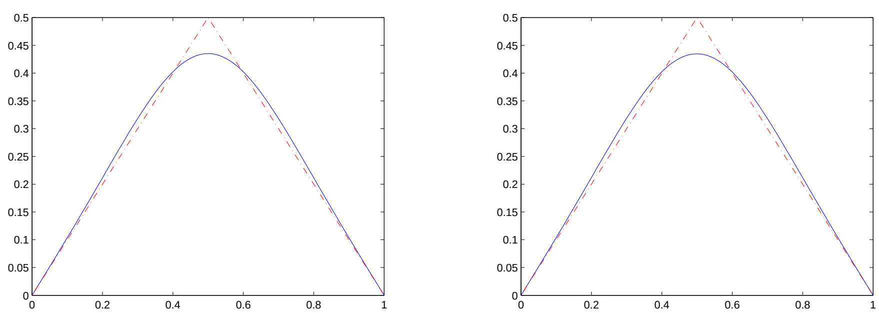

(a) $\delta = 0, \omega = (0.25, 0.75), iter = 20, err = 0.0616$
(b) $\delta = 0.001, \omega = (0.25, 0.75), iter = 20, err = 0.0623$

FIGURE 5. Reconstruction of the initial temperature with singularity in Example 2.

Example 3. In this example, we test a two-dimensional initial profile. For this, we take the exact solution $y(x,y,t)$ and the initial temperature $\mu(x,y)$ as

$$y(x,y,t) = \sin(\pi x)\sin(\pi y)\exp(\sin(\pi t)), \quad \mu(x,y) = \sin(\pi x)\sin(\pi y).$$

The function $f(x,y,t)$ is computed through equation (3.1) using $y(x,y,t)$, the boundary condition $\eta_1(x,y,t) = 0$ on $\Gamma_D \times (0,T)$, $\Gamma_D = \partial\Omega$ while $\Gamma_N = \emptyset$.

The exact initial temperature and the numerically reconstructed one for the H^1 and L^2 observation data are presented in Figure 6 (a), (b) and (c), respectively. The observation region $\omega = (1/4, 3/4) \times (1/4, 3/4)$. We choose the starting measurement time $\tau = 0.1$, which leads to a fast convergence of the reconstruction process. But when the first measurement starts at $\tau = 0.2$ the convergence of the reconstruction process slows down drastically for both the H^1 and L^2 observation data.

Example 4. We take the exact solution $y(x,y,t)$ and the initial temperature $\mu(x,y)$ as

$$y(x,y,t) = \sin(2\pi x)\sin(2\pi y)\exp(\sin(\pi t)), \quad \mu(x,y) = \sin(2\pi x)\sin(2\pi y)$$

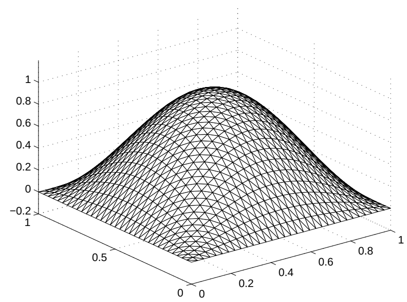

(a) exact initial data.

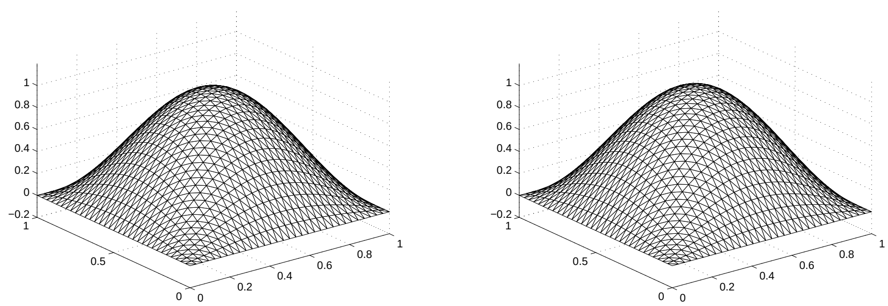

(b) $\tau = 0.1, \delta = 0.01, \gamma = 1E{-}8, iter = 4, err = 0.0463$
(c) $\tau = 0.1, \delta = 0.01, \gamma = 1E{-}9, iter = 4, err = 0.0644$

FIGURE 6. 2D reconstruction in Example 3: (a) exact initial data; (b) H^1-data; (c) L^2-data.

and only measure the L^2-data here. The function $f(x, y, t)$ is computed through equation (3.1) using $y(x, y, t)$, the boundary condition $\eta_1(x, y, t) = 0$ on $\Gamma_D \times (0, T)$, $\Gamma_D = \partial\Omega$ while $\Gamma_N = \emptyset$.

As Figure 7 (a) shows, the exact initial temperature has much oscillation with four extremals (two peaks and two bottoms). In Figure 7 (b) and (c), the numerically reconstructed solutions for two different starting time, $\tau = 0.01$ and 0.02 respectively, are presented for the observation region $\omega = (1/4, 3/4) \times (1/4, 3/4)$. We achieved quite good profiles to the original initial temperature. It is worth noting that although finally the relative error for Figure 7 (b) is only slightly better than Figure 7 (c), but the former one achieves a reasonable profile much faster (10 iterations) than the latter (40 iterations). Next we choose the starting measurement time $\tau = 0.01$ but shift the observation region toward the lower left corner of Ω, i.e., $\omega = (1/8, 5/8) \times (1/8, 5/8)$, one can see that the numerically reconstructed solution achieves much better reconstruction in the lower left region. More specifically, the peak achieves almost full height in the lower left corner as the exact one but the diagonally opposite peak is obviously flatter due to the insufficient measurement data there.

Example 5. This is also a two-dimensional example, but with mixed Dirichlet and Neumann boundary conditions, and the measurement data taken only on part of the boundary. We take the exact solution $y(x, y, t)$ and the initial temperature

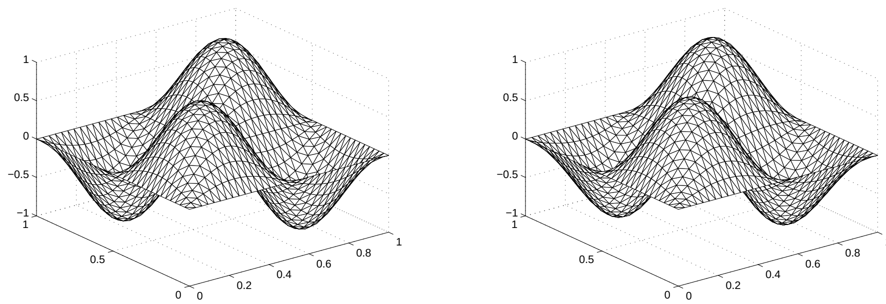

(a) exact initial data.
(b) $\tau = 0.01, \delta = 0.01, \gamma = 1E{-}9, iter = 100, err = 0.0872$

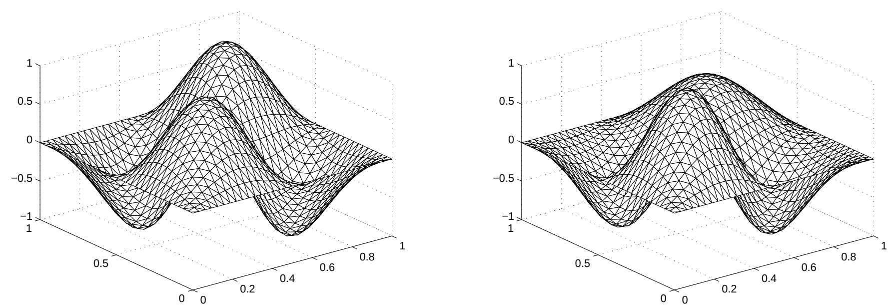

(c) $\tau = 0.02, \delta = 0.01, \gamma = 1E{-}9, iter = 100, err = 0.1701$
(d) $\tau = 0.01, \delta = 0.01, \gamma = 1E{-}9, iter = 100, err = 0.3678$

FIGURE 7. 2D reconstruction in example 4. (a) exact initial data, (b) and (c) comparison with different starting time, τ=0.01 and 0.02 respectively, with measurement in $\omega = (1/4, 3/4) \times (1/4, 3/4)$, (c) and (d) comparison with different positions of the observation regions, $\omega = (1/4, 3/4) \times (1/4, 3/4)$ and $\omega = (1/8, 5/8) \times (1/8, 5/8)$ respectively, with the starting time τ=0.01.

$\mu(x, y)$ as

$$y(x, y, t) = \sin(\pi x)\sin(\frac{y+1}{2}\pi)\exp(\sin(\pi t)), \quad \mu(x, y) = \sin(\pi x)\sin(\frac{y+1}{2}\pi).$$

The function $f(x, y, t)$ is computed through equation (3.1) using $y(x, y, t)$. The mixed boundary conditions are given as in (3.1), with the boundary functions $\eta_2(x, y, t) = 0$ on $\Gamma_N \times (0, T)$ and $\eta_1(x, y, t) = 0$ on $\Gamma_D \times (0, T)$, where $\Gamma_N = (0, 1) \times \{0\}$, $\Gamma_D = \partial\Omega \backslash \Gamma_N$. We take the starting observation time $\tau = 0.02$, but the measurement data of the flux $\partial_n y$ are assumed to be available only on a small part of $\partial\Omega$, namely, Γ_N or part of Γ_N. The reconstruction under such setting is extremely challenging and much harder than all the previously considered cases. But as our theory predicted, we might still have chances to recover a reasonable profile of the initial temperature.

We have plotted the exact initial temperature, the numerically reconstructed ones with different noise level and different size of the measurement region, see Figure 8 (a), (b), (c), (d) and (e), respectively. It is remarkable that one can still achieve satisfactory reconstructions. It is even more amazing to observe that one can reduce the size of the observable region $\omega = \Gamma_N$ till some threshold value but still get rather reasonable approximate reconstruction, see Figure 8 (d) and (e).

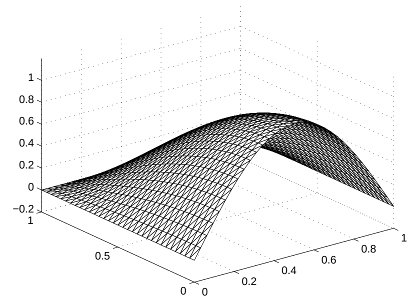

(a) exact initial data.

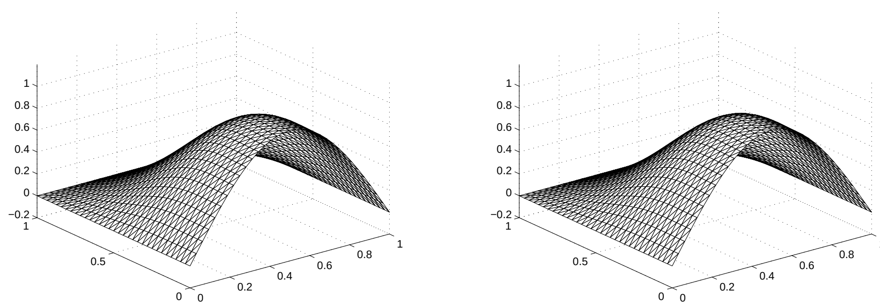

(b) $\delta = 0.001, \gamma = 1E{-}10, iter = 60, err = 0.0618$
(c) $\delta = 0.01, \gamma = 1E{-}10, iter = 60, err = 0.0633$

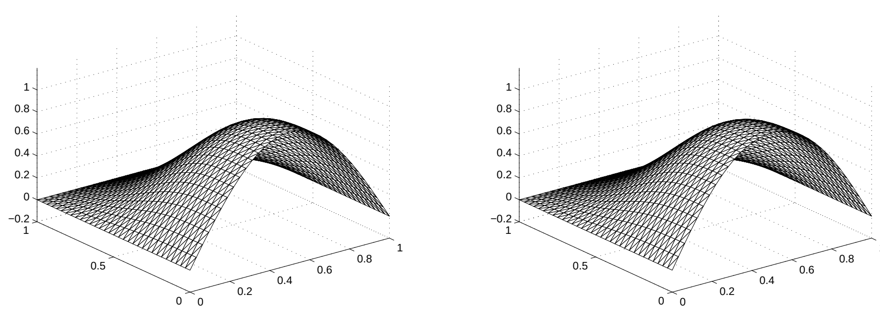

(d) $\omega = (1/8, 7/8), \gamma = 1E{-}10, iter = 60, err = 0.0638$
(e) $\omega = (1/4, 3/4), \gamma = 1E{-}10, iter = 60, err = 0.0651$

FIGURE 8. 2D reconstruction with boundary measurement data in Example 5: (a) exact initial data; (b), (c) reconstruction with L^2 data in $\omega = \Gamma_N = (0,1) \times \{0\}$ with different noise levels; (d), (e) reconstruction with L^2 data of noise level $\delta = 0.01$ with different sizes of the observation region.

REFERENCES

[1] K. A. Ames and B. Straughan, "Non-standard and Improperly Posed Problems," Academic Press, San Diego, 1997.

[2] J. Cheng, M. Yamamoto and J. Zou, *A priori strategy in discretization of the Tikhonov regularization*, In "Progress in Analysis," World Scientific, New Jersey, (2003), 1405–1412.
[3] J. Hadamard, "Lectures on Cauchy Problem in Linear Partial Differential Equations," Yale Univ. Press, New Haven, 1923.
[4] O. Yu. Imanuvilov and M.Yamamoto, *Carleman estimates for a parabolic equation in a Sobolev space of negative order and its applications*, Lecture Notes in Pure Appl. Math., **218** (2001), 113–137.
[5] Y. L. Keung and J. Zou, *Numerical identifications of parameters in parabolic systems*, Inverse Problems, **14** (1998), 83–100.
[6] M. V. Klibanov, *Estimates of initial conditions of parabolic equations and inequalities via the lateral Cauchy data*, Inverse Problems, **22** (2006), 494–514.
[7] M. V. Klibanov and A. Timonov, "Carleman Estimates for Coefficient Inverse Problems and Numerical Applications," VSP, Utrecht, 2004.
[8] M. M. Lavrent'ev, V. G. Romanov and S. P. Shishat·skii, "Ill-posed Problems of Mathematical Physics and Analysis," American Mathematical Society, Providence, RI, 1986.
[9] M. Lees and M. H. Protter, *Unique continuation for parabolic differential equations and inequalities*, Duke Math. J., **28** (1961), 369–382.
[10] J. Li and J. Zou, *A multilevel model correction method for parameter identification*, Inverse Problems, **23** (2007), 1759–1786.
[11] J. L. Lions and E. Magenes, "Non-homogeneous Boundary Value Problems and Applications," Vol. I, Springer-Verlag, Berlin, 1972.
[12] L. E. Payne, "Improperly Posed Problems in Partial Differential Equations," SIAM, Philadelphia, 1975.
[13] A. Pazy, "Semigroups of Linear Operators and Applications to Partial Differential Equations," Springer-Verlag, Berlin, 1983.
[14] S. Saitoh and M. Yamamoto, *Stability of Lipschitz type in determination of initial heat distribution*, J. Ineq. Appl., **1** (1997), 73–83.
[15] L. Scott and S. Zhang, *Finite element interpolation of nonsmooth function satsifying boundary conditions*, Math. Comput., **54** (1990), 483–493.
[16] D. Xu and M. Yamamoto, *Stability estimates in state-estimation for a heat process*, In "Proceedings of the Second ISAAC Congress," Vol. 1 (Fukuoka, 1999): Int. Soc. Anal. Appl. Comput. 7, 193–198, Kluwer Acad. Publ., Dordrecht, 2000.
[17] J. Xu, "Theory of Multilevel Methods," PhD thesis, Cornell University, 1989.
[18] M. Yamamoto and J. Zou, *Simultaneous reconstruction of the initial temperature and heat radiative coefficient*, Inverse Problems, **17** (2001), 1181–1202.
[19] M. Yamamoto and J. Zou, *Conditional stability in reconstruction of initial temperatures*, Proceedings of the 5th ISAAC Congress, World Scientific, New Jersey, 2008, 1385–1390.
[20] G. Yuan and M. Yamamoto, *Lipschitz stability in the determination of the principal part of a parabolic equation*, to appear in ESAIM: COCV.

Received March 2008; revised August 2008.

E-mail address: jzli@math.cuhk.edu.hk
E-mail address: myama@ms.u-tokyo.ac.jp
E-mail address: zou@math.cuhk.edu.hk

UTMS

2008–31 Shigeo Kusuoka: *A certain Limit of Iterated CTE.*

2008–32 Toshio Oshima: *Katz's middle convolution and Yokoyama's extending operation.*

2008–33 Keiichi Sakai: *Configuration space integrals for embedding spaces and the Haefliger invariant.*

2009–1 Tadayuki Watanabe: *On Kontsevich's characteristic classes for higher dimensional sphere bundles II : higher classes.*

2009–2 Takashi Tsuboi: *On the uniform perfectness of the groups of diffeomorphisms of even-dimensional manifolds.*

2009–3 Hitoshi Kitada: *An implication of Gödel's incompleteness theorem.*

2009–4 Jin Cheng, Junichi Nakagawa, Masahiro Yamamoto and Tomohiro Yamazaki: *Uniqueness in an inverse problem for one-dimensional fractional diffusion equation.*

2009–5 Y. B. Wang, J. Cheng, J. Nakagawa, and M. Yamamoto : *A numerical method for solving the inverse heat conduction problem without initial value.*

2009–6 Dietmar Hömberg, Nataliya Togobytska, Masahiro Yamamoto: *On the evaluation of dilatometer experiments.*

2009–7 Toshio Oshima and Nobukazu Shimeno: *Heckman-Opdam hypergeometric functions and their specializations.*

2009–8 Atsushi Yamashita: *Compactification of the homeomorphism group of a graph.*

2009–9 Jingzhi Li, Masahiro Yamamoto, and Jun Zou: *Conditional stability and numerical reconstruction of initial temperature.*

ADDRESS:
Graduate School of Mathematical Sciences, The University of Tokyo
3–8–1 Komaba Meguro-ku, Tokyo 153-8914, JAPAN
TEL +81-3-5465-7001 FAX +81-3-5465-7012